

An autoencoder-based surrogate waveform model for quasi-circular binary-black-hole mergers

Anastasios Theodoropoulos,¹ Nino Villanueva,^{2,1} Osvaldo Gramaxo Freitas,^{3,1} Tiago Fernandes,^{3,1} Solange Nunes,³ Alejandro Torres-Forné,^{1,4} José A. Font,^{1,4} Antonio Onofre,³ and José D. Martín-Guerrero^{2,5}

¹*Departamento de Astronomía y Astrofísica, Universitat de València,
Av. Vicent Andrés Estellés 19, 46100, Burjassot (València), Spain**

²*IDAL, Electronic Engineering Department, ETSE-UV, University of Valencia,
Avda. Universitat s/n, 46100 Burjassot, Valencia, Spain*

³*Centro de Física das Universidades do Minho e do Porto (CF-UM-UP),
Universidade do Minho, 4710-057 Braga, Portugal*

⁴*Observatori Astronòmic, Universitat de València,
Catedràtic José Beltrán 2, 46980, Paterna (València), Spain*

⁵*Valencian Graduate School and Research Network of Artificial Intelligence (ValgrAI), Spain*

(Dated: February 3, 2026)

The generation of accurate waveforms from binary black hole (BBH) mergers is a major effort in Gravitational-Wave Astronomy. In recent years, machine-learning-based surrogate models for BBH waveforms have been proposed. Those offer the potential to dramatically accelerate waveform generation while maintaining accuracy competitive with that of traditional waveform approximants. In this work, we investigate the viability of autoencoders as generative models for gravitational-wave signals from quasi-circular BBH mergers. We introduce **AESur3dq8**, a novel surrogate waveform model based on autoencoders that enables the rapid and accurate construction of large template banks, producing millions of waveforms in under a second using modest computational resources. The model is trained on the numerical-relativity-informed surrogate **NRHybSur3dq8** and subsequently fine-tuned using the SXS catalog of BBH simulations. We demonstrate that waveforms generated by **AESur3dq8** achieve mismatches of order 10^{-4} with respect to Numerical Relativity waveforms, and that parameter estimation performed with these templates yields results fully consistent with those reported by the LIGO–Virgo–KAGRA Collaboration for observed gravitational-wave events.

I. INTRODUCTION

Gravitational waves offer a brand new window to the physical world, complementing the wealth of information collected through the electromagnetic channel. In particular, they provide a unique opportunity to probe gravity and matter in some of the most extreme conditions found in Nature. Their long-awaited detection was made possible by the LIGO [1] and Virgo [2] detectors. The latest release of the Gravitational-Wave Transient Catalog from the LIGO–Virgo–KAGRA (LVK) collaboration has recently updated the number of confident detections to 218 observations, all of them associated with compact binary coalescences, predominantly binary black hole (BBH) mergers [3–7]. As the sensitivity of current detectors is improved [2, 8] and new detectors join the observations [9–11], the amount of gravitational-wave observations is expected to significantly grow. New facilities as the Einstein Telescope or the Cosmic Explorer are expected to achieve detection rates of order 100,000 BBH mergers per year [9, 12]. As a result, accelerating both the detection and parameter estimation capabilities of current pipelines will soon become critical in order to extract accurate results for as many gravitational-wave signals as possible.

Advances will undoubtedly hinge on the efficient and rapid processing of those data, turning Artificial Intelligence and Machine Learning (ML) into key methodological approaches to boost results. Their use, which is already substantial and keeps steadily growing (see [13–16] for recent reviews), is likely going to widespread across all subareas of Gravitational-Wave Astronomy, from the mitigation of the noise of the detectors to the modelling and generation of waveforms of compact binary coalescences, from strategies for detection searches to source classification and astrophysical inferences. In this work, we focus on the problem of gravitational-waveform generation from compact binary coalescences, specifically BBH mergers. The accurate computation of such waveforms is computationally demanding, primarily due to the intrinsic difficulty of solving the equations of motion governing binary systems in General Relativity, whether analytically or numerically. Analytic approaches lose accuracy in the late inspiral and merger phases of compact binary coalescences, where strong-field and tidal effects become dominant, leaving Numerical Relativity as the only viable method for first-principles waveform computation. Although Numerical Relativity has achieved remarkable success, it remains severely limited in its ability to model generic binary configurations, particularly those involving large mass ratios, misaligned spins, or non-quasi-circular (eccentric) orbits. Even for relatively simple systems, Numerical Relativity simulations require substantial computational resources, restricting current catalogs

* anastasios.theodoropoulos@uv.es

to approximately $\mathcal{O}(10^3)$ numerically generated waveforms for BBH systems, and roughly an order of magnitude fewer for binary neutron star systems. In contrast, gravitational-wave searches conducted by the LVK Collaboration typically rely on template banks containing $\mathcal{O}(10^6 - 10^7)$ waveforms. The vast majority of these are generated using so-called approximants, i.e. fast, semi-analytic waveform models that produce accurate predictions as functions of the source's physical parameters. These approximants are commonly calibrated against Numerical Relativity waveform catalogs and have enabled the successful analysis of all gravitational-wave signals detected to date.

More specifically, this investigation focuses on the use of ML models to accelerate the gravitational-waveform generation process. In this context, Gaussian Process Regression has been employed to construct surrogate waveform models for both non-precessing and precessing BBH systems, enabling accurate predictions at regions of parameter space not directly covered by Numerical Relativity [17]. A further example is provided by our previous work [18], in which we introduced a neural-network-based surrogate model, heavily reliant on Principal Component Analysis (PCA), designed to rapidly and accurately generate non-precessing BBH waveforms. When applied to waveform approximant data, this model achieves median reconstruction mismatches of order 10^{-6} to 10^{-4} , depending on the approximant. Correspondingly, median mismatches of order 10^{-5} are obtained when trained on Numerical Relativity datasets. The slight degradation in the latter case is primarily attributable to the limited availability of numerical waveforms for training. Performance benchmarks demonstrate that the PCA-based model of [18] can generate more than one million waveforms in less than 3 milliseconds when deployed on a GPU. Recent studies have further explored the potential of neural networks to enhance the efficiency of surrogate waveform models. For instance, [19] implemented a four-layer neural network to predict the interpolation coefficients in the parameterized surrogate framework originally introduced in [20]. Similarly, [21] adopted the same surrogate methodology but replaced traditional regression techniques with autoencoders. Their analysis uncovered an intriguing “spiral” structure in the latent space, reflecting the dependence of the fitting coefficients on the mass ratio. By exploiting the autoencoder's ability to learn smooth, differentiable mappings between input parameters and surrogate coefficients, the authors achieved faster and more accurate regression. A comprehensive overview of these developments can be found in [15].

Here, we build on our previous investigation [18], developing a new surrogate waveform model dubbed **AESur3dq8** based on autoencoders, which are a generalisation of PCA. Previous work employing autoencoders [21] has focused on non-spinning BBH mergers, for which the mass ratio is the sole input parameter. In this framework, the autoencoders are used primar-

ily as a representation-learning tool. They learn a low-dimensional latent encoding of the waveform data, which subsequently informs a fully connected neural network responsible for generating the final waveform. Both PCA and autoencoders capture the spiral structure found in the coefficient space, with autoencoders providing a somewhat clearer representation. We extend the approach of [21] by using the autoencoder not merely as a representation-learning tool but, through the introduction of an additional fully connected network upstream of the decoder, as a hybrid artificial neural network capable of producing gravitational-wave signals from quasi-circular BBH systems. Moreover, we further extend the model of [21] by incorporating the individual black hole spins as explicit input parameters of the network, in addition to the mass ratio.

The structure of this paper is the following: In Section II we present the methodology to build our datasets. Section III describes our ML model, its specific architectures and the training procedure. In Section IV we discuss the main results of our analysis, namely the accuracy of the generated waveforms and the speed of the generation process as a function of the samples used. Moreover, this section also reports on the parameter estimation of an actual gravitational-wave signal using the BILBY pipeline [22], comparing the posterior distributions of the BBH parameters obtained using our surrogate waveform and a baseline approximant. Finally, Section V presents our conclusions. The surrogate waveform models produced in this work are publicly available¹.

II. DATASETS

Deep Learning frameworks usually require large datasets in order to properly interpolate between the input and output parameter spaces. This becomes a major problem when applying Deep Learning methods in the context of Numerical Relativity, as current catalogs contain at most only a few thousand waveforms [23–29]. Our approach to this problem is to generate a substantial dataset using an existing surrogate model which contains most of the information about what a gravitational-wave signal should look like and then fine-tune the model on our smaller dataset consisting on the Numerical Relativity produced waveforms. This is a widely used technique in the context of object recognition [30], classification, as well as Large Language Models [31]. In this work we focus on BBH coalescence signals, generating the approximant waveforms using the **NRHybSur3dq8** [32, 33] surrogate model. The catalog we use is the SXS catalog², which is publicly available and features a relatively large number of waveforms in the parameter space we want to explore.

¹ <https://github.com/TasosTheodoropoulos/AESur3dq8.git>

² data.black-holes.org

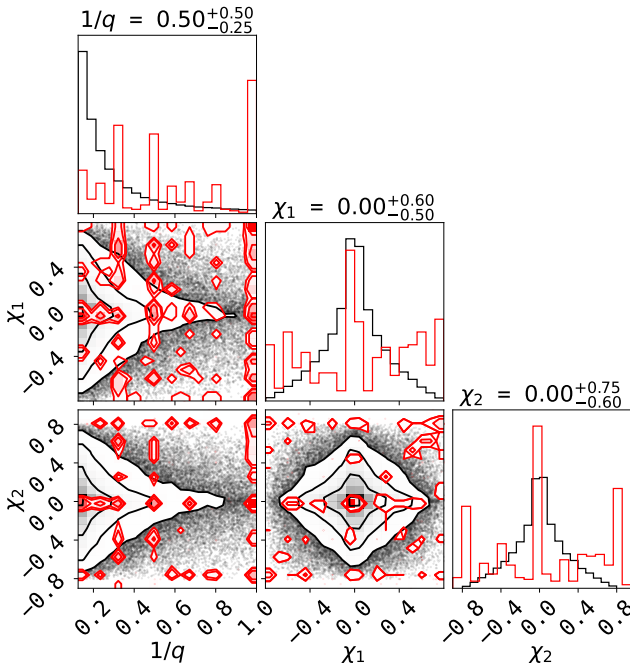


FIG. 1: Corner plot showing the distribution of the parameters of the NRHybSur3dq8 dataset, in gray, and overlaid on top of it, in red, the respective distribution for the SXS dataset. The contour plots display the 0.5, 1, 1.5 and 2σ isocontours, overlayed on top of a scatter plot of the parameters to show the density of points. Note that the points in the regions in-between isocontour levels are not displayed for clarity.

A. Approximant dataset

Using the `GWSURROGATE` [34] python package, we generate 102,400 BBH waveforms for the `NRHybSur3dq8` model. Since we do not want to create an overly complex dataset that will make it difficult for the model to converge, we uniformly sample both the BBH mass ratio $q = M_2/M_1$ in the interval [1,8] and the black hole individual spins χ_1, χ_2 , in the interval [-0.8, 0.8]. Those are assumed to be aligned with the orbital angular momentum, since we only consider non-precessing, quasi-circular BBH mergers in this work. We note that we uniformly sample in mass ratios and spins in order to avoid biases by oversampling specific regions of the parameter space. Another important remark is that we uniformly sample in the magnitude of χ_1, χ_2 and then we sample again using the `bilby.gw.prior.AlignedSpin` class of the `BILBY` package, thus resulting in non-uniform χ_1, χ_2 distributions. Those distributions are displayed in Fig. 1.

In a more technical note, the waveforms are generated in simulation units; the amplitudes/phases are scaled by the sum of the Christodoulou masses of both black holes and the sampling rate used is $2M_\odot^{-1}$. At the time of BBH merger we use the time corresponding to the maximum amplitude of the quadrupolar gravitational-wave

mode $(l, |m|) = (2, 2)$ and we line up the waveforms such that the merger is located in time $100M_\odot$ before the end of the window, which we choose to have a duration of $4096M_\odot$. Lastly, we further simplify the problem by setting the initial phase of all waveforms to zero. Using the `train_test_split` function [35] and a 81/10/9 train/test/validation split on our dataset, we obtain the sets used for training, testing and validation of our network. This results in sets with 82944, 10240, and 9216 waveforms, respectively.

TABLE I: Detailed neural network architecture for the encoder, decoder and mapping network, containing the type, number of neurons and activation function for each layer.

Component	Layer	Units	Activation
Encoder	Input	2048	—
	Dense 1	1024	Leaky ReLU
	Dense 2	512	Leaky ReLU
	Dense 3	256	Leaky ReLU
	Dense 4	128	Leaky ReLU
	Latent (Output)	64	Linear
Decoder	Input (Latent)	64	—
	Dense 1	128	Leaky ReLU
	Dense 2	256	Leaky ReLU
	Dense 3	512	Leaky ReLU
	Dense 4	1024	Leaky ReLU
	Output	2048	Linear
Mapping Network	Input (Parameters)	3	—
	Dense 1	128	Leaky ReLU
	Dense 2	512	Leaky ReLU
	Dense 3	512	Leaky ReLU
	Dense 4	128	Leaky ReLU
	Output (Latent)	64	Linear

B. Numerical Relativity waveforms

Using the publicly available BBH simulation dataset from the SXS collaboration [36], which contains 2018 simulations, we extract only the $l = m = 2$ modes with the `SXS` python package [37]. Then, we filter these waveforms to make sure they match the parameters of our approximant dataset. We first make sure that we use waveforms that are longer than $4096M_\odot$. Then, we filter out all the waveforms with an effective precessing spin $\chi_p > 0.001$, and mass ratios $q > 8$. Lastly, by making sure that gravitational-wave memory effects are not present, discarding waveforms with final amplitudes higher than a threshold value of 10^{-2} , we end up with 377 waveforms which we interpolate using cubic splines and trim to the desired length ($4096M_\odot$). The parameter distributions for both datasets are shown in Fig. 1. We split our numerical relativity dataset in the same way we did for the `NRHybSur3dq8` dataset, resulting in train/test/validation sets with 305, 38 and 34 numerical waveforms, respectively.

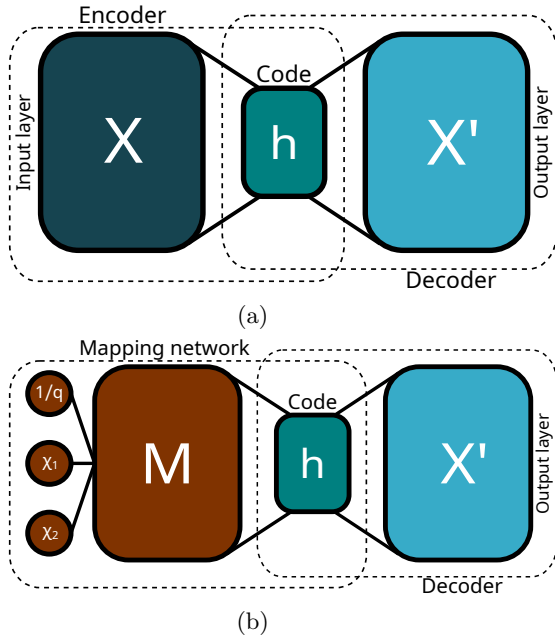


FIG. 2: Schematic representations of the two model configurations used in this work. (a) The autoencoder architecture, consisting of the encoder, decoder, and the latent (code) space. (b) The generative model, obtained by removing the encoder and adding a fully connected network that maps the physical parameters to the latent space.

III. METHODOLOGY

The methodology we employ to generate new waveforms from the initial BBH parameters includes a mix of neural network architectures and training processes which we present in the following subsections.

A. Dimensionality reduction

The need for dimensionality reduction techniques comes from what is commonly referred to as the ‘curse of dimensionality’, which refers to the observation that data get sparser in higher dimensions [38]. As a result, models tend to overfit the data in order to achieve better accuracy or they tend to have redundant and/or correlated variables [39, 40]. To circumvent this issue one can either find more data so that a bigger part of the sparse regions can be covered, select some of the features of the original data, or even extract the most relevant features. In our case, since Numerical Relativity simulations of BBH mergers are computationally intensive, we cannot follow the first option. Moreover, as we want our model to be as accurate as possible we cannot use the second option either. Thus, we employ feature extraction techniques. Some commonly used such techniques are Random Forests [41], PCA and autoencoders. In [18] we

focused on the generation of surrogate BBH waveforms using PCA. Here, we explore the use of autoencoders as the natural nonlinear generalisation of our previous work.

B. Architectures

An autoencoder is an unsupervised learning method, which uses a “bottleneck” architecture, as seen schematically in Fig. 2a, where the input parameters get gradually encoded to less and less parameters until a preferable “compression” or encoding of the input data is reached. Then, a symmetric architecture is employed as the decoder network, shown in Fig. 2b, to “decompress” the encoded version of our data back to their original form. In this work, we adopted a 64-dimensional latent space, corresponding to a compression factor of 32. Our tests indicated that this choice provides the best trade-off between high reconstruction accuracy while avoiding overfitting to the waveform approximant dataset. We also employed an \mathcal{L}_2 -norm `activity_regularizer` in the latent space layer which improved our overall results and helped the mapping network converge to more accurate results.

Fig. 2 illustrates the model configurations used for the development of the surrogate model, the autoencoder itself and the full model which is built from the decoder part and a mapping network. The detailed architectures of the encoder, decoder and mapping network are reported on Table I. All the hidden layers use the `LeakyReLU` activation function, defined as

$$f(x) = \begin{cases} x, & \text{if } x \geq 0 \\ \alpha x, & \text{otherwise} \end{cases} \quad (1)$$

where $\alpha \in (0, 1)$. For $\alpha = 0$ the `LeakyReLU` reduces to the `ReLU` activation function, while in our case we use the default value $\alpha = 0.3$. On the other hand, for the input, output and latent layers we employ a linear activation function, $f(x) = x$. To convert the autoencoder into a generative model, we replace the encoder with a fully connected mapping network that projects the initial parameters into the latent space. These latent representations are then used as inputs to the decoder to generate the corresponding gravitational waveforms. The final architecture is shown in Fig. 2b.

The loss function we use is the Mean Absolute Error (MAE),

$$\mathcal{L} = \frac{1}{N} \sum_i^N (|X_{\text{true}}^i - X_{\text{predicted}}^i|), \quad (2)$$

where $X_{\text{predicted}}^i$ is the output of the model, X_{true}^i is the true value from the training dataset, and the difference of the two is summed over the batch size N .

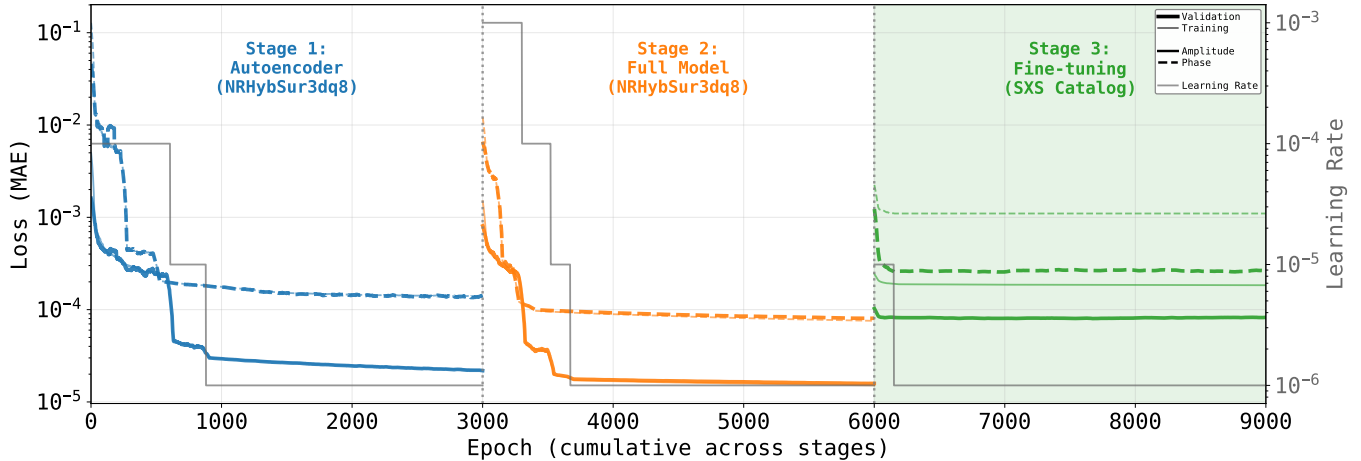


FIG. 3: Loss functions of our models in all three stages of training. From left to right we show the 50-epoch average of the value of the loss and validation loss for each model (amplitude and phase, depicted in solid and dashed lines, respectively) during the autoencoder training with the NRHybSur3dq8 dataset, the full model training with the same dataset, and the full model training with the SXS dataset (fine-tuning stage). We also overlay the LR for each epoch, showing more clearly that the model benefits from the LR scheduler, since the loss function improves at each step.

C. Training

We start the summary of the training procedure by stating the goal of the final model. We need the model to generate gravitational waveforms for quasi-circular BBH mergers given only their mass ratio and their individual spins, (q, χ_1, χ_2) . Since we observed that training the autoencoder on the amplitude and phase components separately, rather than on the full complex waveform, leads to faster convergence and higher accuracy, the first step in our procedure is to split the dataset into unwrapped amplitudes and phases,

$$h = h_+ - i h_\times = A e^{i\phi}, \quad (3)$$

where h is the strain, and h_+ , h_\times its components (the “plus” and “cross” polarizations), A is the amplitude, and ϕ is the phase. The three stages of the training procedure are as follows:

1. We train both autoencoders with the NRHybSur3dq8 dataset; the first one with the amplitudes A and the second one with the phases ϕ . In this way we obtain the reduced representations we need for the next stages.
2. Keeping only the decoder part of the resulting autoencoders, we add a fully-connected network to map the physical parameters to the reduced representations. The ensuing models can predict the amplitude and phase of a waveform given the initial parameters of the system.
3. The last stage entails the fine tuning of the full models, which is performed by retraining them with the Numerical Relativity dataset using a smaller initial Learning Rate (LR).

All three stages of training take 3000 epochs to complete. We use the Adam optimiser with an initial 10^{-4} LR for the first stage and a 10^{-3} LR for the full model training. For the fine-tuning stage, as it is commonly done, we choose a smaller 10^{-5} LR. We also employ a LR scheduler (ReduceLROnPlateau) which checks the validation loss for each epoch. If it does not improve for a specified number of epochs (LR patience), it reduces the LR by a specified factor (LR reduction factor).

The evolution of the loss functions during each training stage and for each model is displayed in Fig. 3. We can see that the training concluded with the models having converged in all stages. We do not observe any overfitting as a validation loss higher than the corresponding training loss would suggest. Also, the use of a LR scheduler is justified by the improvement of the loss functions at each step. It is worth noting that, during the fine-tuning stage, we experimented with k-fold cross-validation and weight averaging across the models trained on each fold, following the approach used in our previous work [18]. However, this strategy did not lead to any improvement in performance. Each epoch takes 1 second to complete when the model is trained with the approximant dataset and with a batch size of 1024 on an NVIDIA RTX 4090 GPU. The fine tuning epochs took much less time, in the order of milliseconds, which is expected from the number of available waveforms. A summary of the model hyperparameters is reported on Table II.

IV. RESULTS

We turn now to discuss our results when testing the accuracy of our autoencoder-based model inside its training parameter space, along with the time they take to make

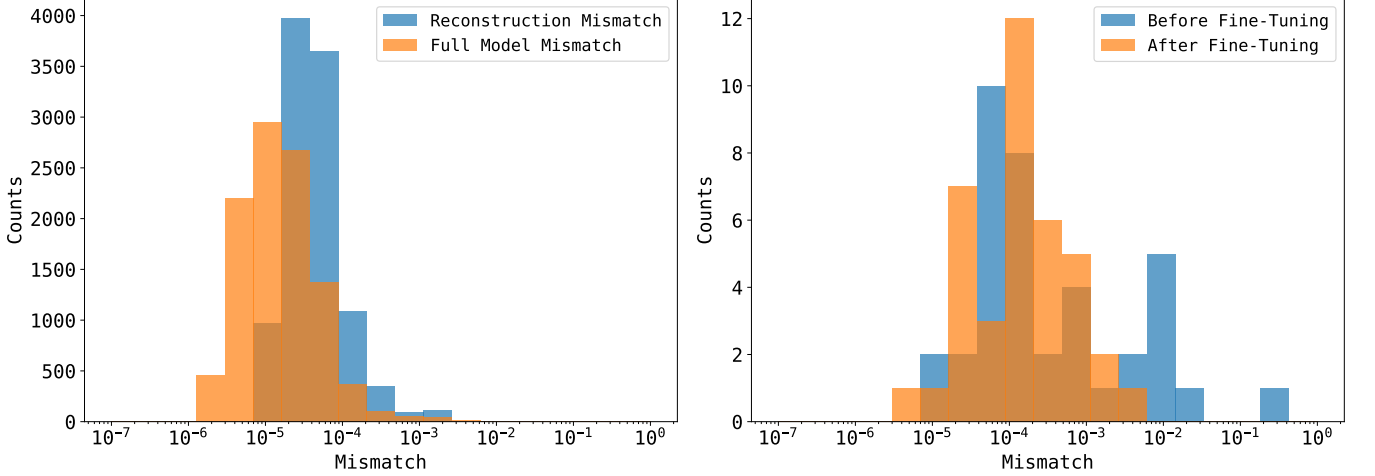


FIG. 4: Mismatch distributions for the model-generated waveforms. Left: distribution for the autoencoder reconstruction of the NRHybSur3dq8 test set overlaid with mismatches from waveforms generated by the full model trained on the same dataset. Right: distribution between waveforms generated by the full model and the SXS test set, shown before and after fine-tuning.

TABLE II: Summary of the key hyperparameters used during the training procedure, where AE, Full, and FT refer to the autoencoder, the full model and the fine tuning stage, respectively.

Parameter	Value
Optimizer	Adam
Learning rate	10^{-4} (AE), 10^{-3} (Full), 10^{-5} (FT)
Loss function	Mean Absolute Error
Batch size	1024
Training epochs	3000 (each stage)
LR scheduler	ReduceLROnPlateau
LR reduction factor	0.1
LR patience	250 (AE), 125 (Full, FT)

an inference, and how this time scales with the number of points. We use BILBY for the parameter estimation tests [22]. An inference is carried out for an illustrative BBH gravitational-wave signal detected by the LVK collaboration. To assess the accuracy of our model we employ the mismatch \mathcal{M} , a metric commonly used in the literature for the assessment of similarity between generated and real waveforms. The mismatch is related to the overlap \mathcal{O} by

$$\mathcal{M}(h, \hat{h}) = 1 - \mathcal{O}(h, \hat{h}) = 1 - \frac{\langle h | \hat{h} \rangle}{\sqrt{\langle h | h \rangle \langle \hat{h} | \hat{h} \rangle}}, \quad (4)$$

where

$$\langle h | \hat{h} \rangle = 4 \operatorname{Re} \int_{-\infty}^{\infty} \tilde{h}(f) \tilde{h}^*(f) df \approx 4 \operatorname{Re} \sum_k \tilde{h}_k \tilde{h}_k^* \Delta f, \quad (5)$$

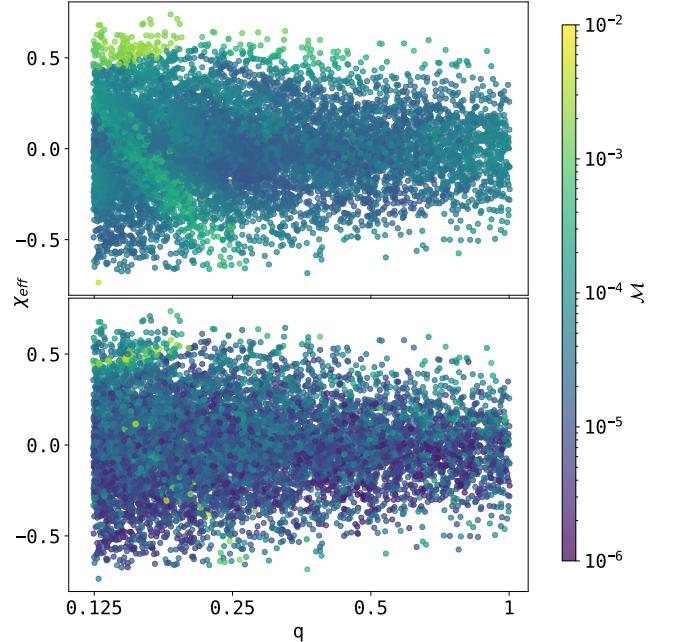


FIG. 5: Scatter plot of the distribution of the physical parameters of the NRHybSur3dq8 test dataset, with the spins combined into the effective spin $\chi_{\text{eff}} = \frac{\chi_1 + q\chi_2}{1+q}$ and coloured with the mismatch between the predicted waveform and the real one corresponding to each parameter combination. The top panel displays the autoencoder's reconstruction mismatches at the conclusion of the first training stage, whereas the bottom panel shows the mismatches for the full model at the end of the second stage.

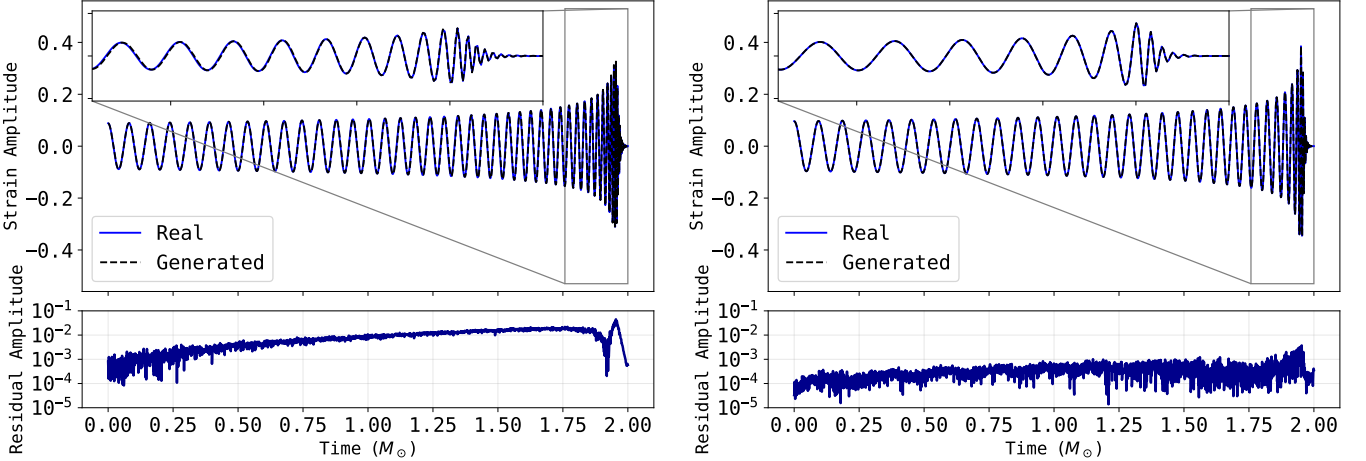


FIG. 6: Visualization of waveforms generated by our model, overlaid with the corresponding numerical-relativity waveforms to illustrate the model’s performance. Even under close inspection (see insets), the generated waveforms are visually indistinguishable from the true waveforms. The left panel shows the waveform with the highest mismatch in the test set, $\mathcal{M} = 3.94 \times 10^{-3}$, while the right panel shows the waveform with the lowest mismatch, $\mathcal{M} = 7 \times 10^{-6}$. The lower subpanels display the amplitude residuals between the generated and true waveforms.

A. Accuracy

For every waveform in the approximant test set we generate a waveform using our model and its initial parameters. Then, using Eq. (4), we calculate the similarity between them. We repeat the same process for our test split of the SXS dataset before and after we fine-tune our model. The results of these tests are summarised in Table III and are displayed in the histograms shown in Fig. 4 and in the scatter plot of Fig. 5.

The mean mismatch obtained for the approximant dataset is of the order of 10^{-5} while for the SXS dataset the accuracy degrades by about one order of magnitude. The maximum mismatch values attained are associated with the non-negligible tails seen in the histograms of Fig. 4. This is also illustrated in Fig. 5 which shows the correlation of the physical parameters of the binary with the mismatch, highlighting regions of significant mismatch in the parameter space. In particular, the tests with numerical-relativity waveforms (right plot of Fig. 4) show a much more pronounced high-mismatch tail than those based on the approximant dataset (Fig. 4, left plot). This particularly manifests for the results where no fine-tuning has been applied. In such case, the waveform with the worst reconstruction shows a mismatch of about 30% which would render the model unusable as a surrogate. However, the fine-tuning stage significantly reduces the impact of the high mismatch tail and improves the overall performance of the model. Indeed, the mean mismatch values improve by more than an order of magnitude after the fine-tuning stage. This makes our model accurate enough to be used as a surrogate waveform generation model. This is illustrated in Fig. 6 where we display the

TABLE III: Summary of the accuracy of the model with the two datasets used. Both the mean and the maximum values of the mismatch are reported.

Model	Dataset	Mean	Max
Autoencoder	NRHybSur3dq8	8.56×10^{-5}	3.85×10^{-3}
Full	NRHybSur3dq8	4.43×10^{-5}	6.00×10^{-3}
Full	SXS	9.69×10^{-3}	2.82×10^{-1}
Fine-tuned	SXS	3.97×10^{-4}	3.94×10^{-3}

waveform with the worst mismatch in the SXS dataset after fine-tuning, $\mathcal{M} = 3.94 \times 10^{-3}$, along with the one with the best mismatch. No significant differences are observed even when zooming in in the merger part of the signal. The lower panels of the same figure show the amplitude residuals between the actual and generated waveforms. In both cases, the residuals increase toward merger, where the amplitude varies more rapidly. This effect is more pronounced in the left lower panel which corresponds to the waveform with the highest mismatch.

Despite the overall accuracy of the results, Fig. 5 shows, again, that two regions with high mismatch values are present in both datasets. We note that those regions (correlated with the tails in the histograms) are also present in our PCA-base model (see Fig. 7 in [18]). The structures observed in the scatter plot seem to be somehow bound to the specific NRHybSur3dq8 approximant but its origin, however, is unclear and needs further analysis. It is worth pointing out that the mapping network along with the retraining of the decoder seems to help the model improve the predicted waveforms by an order of magnitude, notably alleviating a big part of the high mismatch areas, as seen in the bottom panel of

Fig. 5.

B. Speed

We now discuss the time it takes the model to generate waveforms for different number of samples. In order to measure this time we take the following steps:

1. Compile the model by doing a computation with a small number of samples.
2. Perform 3 warm-up computations with an actual sample size, to get rid of “outliers” from the first computation.
3. Perform 10 computations with different number of samples.

In this way, we ensure that neither model initialization nor random time delays affect the speed measurement, yielding an unbiased assessment of the model’s performance in waveform generation and its scalability with the number of samples. We also make use of batches, since as the number of samples increases the weights and the outputs of the neurons do not fit any more in GPU memory and the model fails to run. With the use of a batch size of $\min(10000, \text{Number of samples})$ we make sure that the model runs correctly with our available GPU memory (NVIDIA RTX 4090). Having higher usable GPU memory would allow running larger batches and thus speeding up the total waveform generation time, as the forward pass itself is a very rapid and parallelisable task on GPUs.

Our results are summarised in Table IV. We benchmarked our model using both its serialised just-in-time (JIT) version and its implementation within the GWSURROGATE package, enabling a fair comparison with the NRHybSur3dq8 approximant. We find that GWSURROGATE introduces substantial overhead, increasing CPU waveform generation times by roughly one order of magnitude and up to a factor of 240 on GPUs for large sample sizes. Despite this, even the CPU implementation of our model remains significantly faster than NRHybSur3dq8, making it suitable for low-latency parameter estimation. GPU acceleration provides additional gains for the JIT version as the number of samples increases; however, these gains are negated in the GWSURROGATE implementation due to its high overhead. We also note that NRHybSur3dq8 is run sequentially, as parallel execution on 32 CPU cores resulted in slower performance. Finally, it is worth pointing out that our PCA-based surrogate [18] substantially outperforms AESur3dq8, generating 10 million waveforms in under 40 ms, primarily due to the simplicity of the inverse PCA transform compared to the more complex decoder network.

TABLE IV: Mean waveform generation time (ms) for both versions of our model on CPUs and GPUs across different sample sizes, compared with NRHybSur3dq8 implemented in the GWSURROGATE package. The values with an asterisk are extrapolated using the sample/s values from the previous computation as it does not change with time.

Samples	Raw timing		GWSURROGATE		
	CPU	GPU	CPU	GPU	baseline
10^2	3.1	1.1	10	7.7	520
10^3	16	7.8	93	73	5,200
10^4	66	11	880	820	51,500
10^5	720	40	8,700	8,300	515,000*
10^6	7,200	340	87,000*	83,000*	$5.1 \times 10^6*$

C. Parameter estimation

Having established the accuracy of the surrogate waveforms generated with our autoencoder-based model we turn now to test its capabilities for gravitational-wave parameter estimation. To do so we employ Bayesian inference with nested sampling [42], the most common algorithm for parameter estimation in gravitational-wave data analysis. Nested sampling relies in repeatedly evaluating a likelihood function that requires waveforms. Usually, these waveforms are obtained from surrogate models or approximants, and the speed of the waveform generation stage affects greatly the overall speed of the parameter estimation algorithm. As discussed before, our model shows a significant speedup compared with NRHybSur3dq8. Therefore, we expect a comparable speedup relative to NRHybSur3dq8 in parameter estimation via nested sampling when using our model.

We conduct this test by performing two parameter estimation runs with the BILBY (v2.7.1) Bayesian inference package [22] and the NESSAI (v0.15) sampler [43], one using the NRHybSur3dq8 surrogate model and the other using our method. Since BILBY is built on CPUs we cannot leverage the speedup provided by parallel computing for assessing the benefits of using our model. Hence, all tests presented in this section were performed on CPUs, specifically on an Intel Xeon Platinum 8160 processor running at 2.10 GHz with 24 cores. For its usage in BILBY, our fine-tuned neural network was compiled using JIT compilation and wrapped using GWSURROGATE (v1.1.8) for projecting the waveform in the sky and rescaling it in SI units. Then, we ran the sampler on the real strain data containing the GW200311_115853 event from both of LIGO’s interferometers data along with Virgo data. This event was selected to allow a direct comparison with the results presented in [18] using our PCA-based approach.

An overlapping corner plot showing the obtained results on top of each other is provided in Fig. 7. We can see that the medians obtained by our run lie well within the confidence intervals published by the LVK collabora-

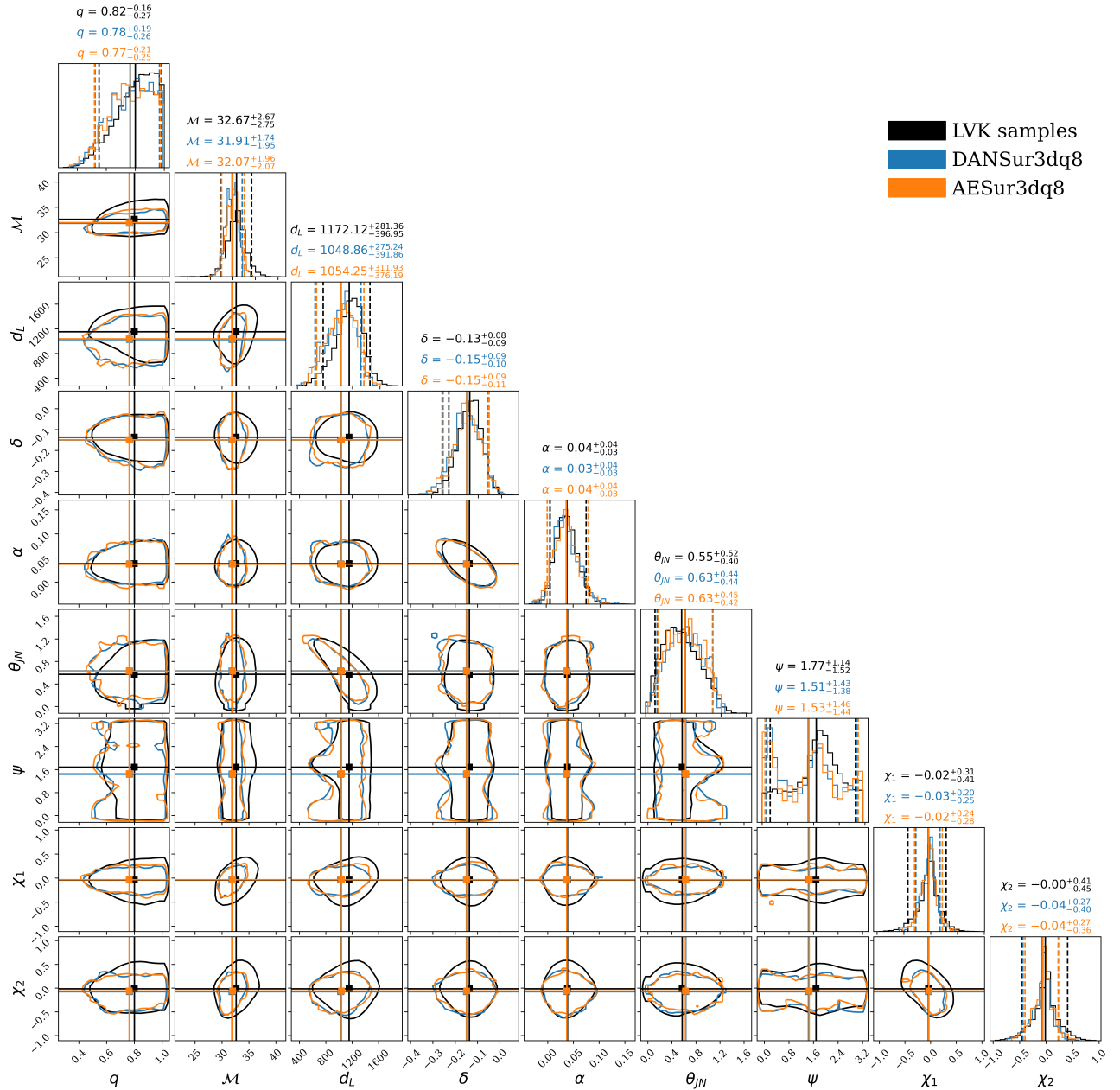


FIG. 7: Results comparison between a parameter estimation run using our model and the results published by the LVK collaboration for the GW200311_115853 event. The published results are outlined in black, our results are represented in blue and the results obtained from the PCA-based model are shown in orange. The magnitudes estimated are, from left to right, the binary mass ratio, the chirp mass, the luminosity distance, the sky localization angles (declination and right ascension), orbital inclination, polarization angle and the spin z -component magnitudes for each object. All estimated medians of the distributions obtained with our model lie within the LVK uncertainty bounds and the obtained distributions correlate fairly well visually. Our results present some multimodality in the polarization angle, probably due to the fact that our model only produces the $l = m = 2$ multipole. We would expect this multimodal distribution to collapse into a unimodal one when higher order multipoles are included in the model.

ration, while the distribution shapes visually correlate fairly well with the exception of the polarization angle, which presents some multimodality which is not present in the LVK samples. This could probably be due to the fact that our model only produces the dominating mul-

tipole. This condition leaves out crucial information for breaking the multimodality in the polarization angle. We also observe that the inferred parameters are distributed very similarly when using either of the two approaches, based on PCA or autoencoders. In terms of inference

time, our model is supposed to enhance the speed of the sampling time specifically. In BILBY’s logging system, the sampling time is computed separately from other parts of the algorithm, providing a value for the speedup of our approach. When obtaining the results presented in this subsection, sampling through the `NRHybSur3dq8` took approximately 12 minutes and 29 seconds, while using our fine-tuned model it took approximately 3 minutes and 33 seconds, providing around a factor 4 speedup. For completeness, with 1000 live points, the PCA-based algorithm run took 3 minutes and 35 seconds to complete, with 346,596 likelihood evaluations accounting for 15.8 seconds of that time.

V. CONCLUSIONS

Machine-learning-based surrogate waveform models have been shown to significantly accelerate waveform generation while achieving levels of accuracy comparable to those of traditional waveform approximants (see e.g. [18]). In this paper we have investigated the viability of artificial neural networks with an autoencoder-based training strategy to generate an efficient reduced representation of gravitational-wave signals from quasi-circular BBH mergers. This work extends our previous study [18], in which we performed a similar assessment using a neural-network-based surrogate model built upon a reduced PCA basis of approximant waveforms.

Our autoencoder-based surrogate waveform model `AESur3dq8` is capable of rapidly generating large template banks, producing millions of waveforms in under a second on GPUs using modest computational resources. Even on standard CPUs, `AESur3dq8` can perform the same task in under 10 seconds. The model training relies on a three-stage procedure. As a first step, we train an autoencoder on the `NRHybSur3dq8` approximant dataset to obtain a reduced, low-dimensional representation of the waveforms. Next, we repurpose the resulting decoder by introducing a mapping network before its input and train the combined system as a single network, again using the `NRHybSur3dq8` dataset. This procedure transforms the autoencoder into a hybrid artificial neural network that can generate gravitational-wave signals from quasi-circular BBH systems. Finally, the model is fine-tuned using the SXS Numerical Relativity dataset, which substantially enhances its accuracy, improving waveform mismatches by approximately two orders of magnitude. In the last part of this paper we have shown that the parameter inference performed using templates generated by `AESur3dq8` leads to fully consistent results with those reported by the LVK Collaboration and with those using our PCA-based model [18] for the gravitational-wave event GW200311-115853, used as an illustrative example.

ACKNOWLEDGMENTS

AT acknowledges support from the Universitat de València through the Atracció de Talent fellowship. NVE is supported by the Valencian Government Grant No. CIAICO/2024/111 and the Spanish Ministry of Economic Affairs and Digital Transformation through the QUANTUM ENIA project call – Quantum Spain project, and the European Union through the Recovery, Transformation and Resilience Plan – NextGenerationEU (Digital Spain 2026) Agenda. OGF is supported by the Portuguese Foundation for Science and Technology (FCT) through doctoral scholarship UI/BD/154358/2022. TF is supported by FCT through doctoral scholarship 2023.03753.BD. OGF, TF, SN and AO acknowledge financial support by CF-UM-UP through the Strategic Fundings UIDB/04650/2020, UIDP/04650/2020, UID/PRR/04650/2025 and UID/04650/2025 of FCT. JAF and ATF are supported by the Spanish Agencia Estatal de Investigación (grant PID2024-159689NB-C21) funded by MICIU/AEI/10.13039/501100011033 and by FEDER/EU, by the Generalitat Valenciana (Prometeo grant CIPROM/2022/49), and by the European Horizon Europe staff exchange (SE) programme HORIZON-MSCA-2021-SE-01 (grant NewFunFiCO-101086251). JDMG is partially supported by the agreement funded by the European Union, between the Valencian Ministry of Innovation, Universities, Science and Digital Society, and the network of research centers in Artificial Intelligence (Valencian Foundation valgrAI), as well as the Valencian Government grant with reference number CIAICO/2024/111; the Spanish Ministry of Economic Affairs and Digital Transformation through the QUANTUM ENIA project call – Quantum Spain project, and the European Union through the Recovery, Transformation and Resilience Plan – NextGenerationEU within the framework of the Digital Spain 2025 Agenda. The authors gratefully acknowledge the computer resources at Artemisa and the technical support provided by the Instituto de Física Corpuscular, IFIC (CSIC-UV). Artemisa is co-funded by the European Union through the 2014-2020 ERDF Operative Programme of Comunitat Valenciana, project IDIFEDER/2018/048. This material is based upon work supported by NSF’s LIGO Laboratory which is a major facility fully funded by the National Science Foundation, as well as the Science and Technology Facilities Council (STFC) of the United Kingdom, the Max-Planck-Society (MPS), and the State of Niedersachsen/Germany for support of the construction of Advanced LIGO and construction and operation of the GEO600 detector. Additional support for Advanced LIGO was provided by the Australian Research Council. Virgo is funded, through the European Gravitational Observatory (EGO), by the French Centre National de Recherche Scientifique (CNRS), the Italian Istituto Nazionale di Fisica Nucleare (INFN) and the Dutch Nikhef, with contributions by institutions from Belgium, Germany, Greece, Hungary, Ireland,

Japan, Monaco, Poland, Portugal, Spain. KAGRA is supported by Ministry of Education, Culture, Sports, Science and Technology (MEXT), Japan Society for the Promotion of Science (JSPS) in Japan; National

Research Foundation (NRF) and Ministry of Science and ICT (MSIT) in Korea; Academia Sinica (AS) and National Science and Technology Council (NSTC) in Taiwan.

-
- [1] B. P. Abbott *et al.* (LIGO Scientific, Virgo), Observation of Gravitational Waves from a Binary Black Hole Merger, *Phys. Rev. Lett.* **116**, 061102 (2016), arXiv:1602.03837 [gr-qc].
- [2] F. Acernese *et al.* (VIRGO), Advanced Virgo: a second-generation interferometric gravitational wave detector, *Class. Quant. Grav.* **32**, 024001 (2015), arXiv:1408.3978 [gr-qc].
- [3] B. P. Abbott and others, GWTC-1: A Gravitational-Wave Transient Catalog of Compact Binary Mergers Observed by LIGO and Virgo during the First and Second Observing Runs, *Physical Review X* **9**, 10.1103/physrevx.9.031040 (2019).
- [4] R. Abbott and others, GWTC-2: Compact Binary Coalescences Observed by LIGO and Virgo During the First Half of the Third Observing Run, *Phys. Rev. X* **11**, 021053 (2021).
- [5] R. Abbott and others, GWTC-3: Compact Binary Coalescences Observed by LIGO and Virgo During the Second Part of the Third Observing Run, arXiv e-prints 10.48550/arXiv.2111.03606 (2021).
- [6] R. Abbott and others, GWTC-2.1: Deep Extended Catalog of Compact Binary Coalescences Observed by LIGO and Virgo During the First Half of the Third Observing Run, *Phys. Rev. D* **109**, 022001 (2024).
- [7] A. G. Abac *et al.* (LIGO Scientific, VIRGO, KAGRA), GWTC-4.0: Constraints on the Cosmic Expansion Rate and Modified Gravitational-wave Propagation, (2025), arXiv:2509.04348 [astro-ph.CO].
- [8] T. L. S. Collaboration, J. Aasi, and others, Advanced LIGO, *Classical and Quantum Gravity* **32**, 074001 (2015).
- [9] E. D. Hall, Cosmic Explorer: A Next-Generation Ground-Based Gravitational-Wave Observatory, *Galaxies* **10**, 10.3390/galaxies10040090 (2022).
- [10] M. Maggiore *et al.* (ET), Science Case for the Einstein Telescope, *JCAP* **03**, 050, arXiv:1912.02622 [astro-ph.CO].
- [11] A. Abac *et al.* (ET), The Science of the Einstein Telescope, (2025), arXiv:2503.12263 [gr-qc].
- [12] M. Branchesi, M. Maggiore, D. Alonso, C. Badger, B. Banerjee, F. Beirnaert, E. Belgacem, S. Bhagwat, G. Boileau, S. Borhanian, D. D. Brown, M. Leong Chan, G. Cusin, S. L. Danilishin, J. Degallaix, V. De Luca, A. Dhani, T. Dietrich, U. Dupletsas, S. Foffa, G. Franciolini, A. Freise, G. Gemme, B. Goncharov, A. Ghosh, F. Gulminelli, I. Gupta, P. Kumar Gupta, J. Harms, N. Hazra, S. Hild, T. Hinderer, I. Siong Heng, F. Iacovelli, J. Janquart, K. Janssens, A. C. Jenkins, C. Kalaghatgi, X. Koroveshi, T. G. Li, Y. Li, E. Lofredo, E. Maggio, M. Mancarella, M. Mapelli, K. Martinovic, A. Maselli, P. Meyers, A. L. Miller, C. Mondal, N. Muttoni, H. Narola, M. Oertel, G. Oganesyan, C. Pacilio, C. Palomba, P. Pani, A. Pasqualetti, A. Perego, C. Périgois, M. Pieroni, O. J. Piccinni, A. Puecher, P. Puppo, A. Ricciardone, A. Riotti, S. Ronchini, M. Sakellariadou, A. Samajdar, F. Santoliquid, B. Sathyaprakash, J. Steinlechner, S. Steinlechner, A. Utina, C. Van Den Broeck, and T. Zhang, Science with the einstein telescope: a comparison of different designs, *Journal of Cosmology and Astroparticle Physics* **2023** (07), 068.
- [13] E. Cuoco *et al.*, Enhancing Gravitational-Wave Science with Machine Learning, *Mach. Learn. Sci. Tech.* **2**, 011002 (2021), arXiv:2005.03745 [astro-ph.HE].
- [14] V. Benedetto, F. Gissi, G. Ciaparrone, and L. Troiano, Applications of machine learning to gravitational wave detection, *Applied Sciences* **13**, 9886 (2023).
- [15] N. Stergioulas, Artificial intelligence and machine learning in gravitational wave astronomy: A review, arXiv preprint (2024), arXiv:2401.07406.
- [16] E. Cuoco, M. Cavaglià, I. S. Heng, D. Keitel, and C. Messenger, Applications of machine learning in gravitational-wave research with current interferometric detectors: Applications of machine learning in gravitational-wave..., *Living Reviews in Relativity* **28**, 2 (2025), arXiv:2412.15046 [gr-qc].
- [17] D. Williams, I. S. Heng, J. Gair, J. A. Clark, and B. Khamesra, Precessing numerical relativity waveform surrogate model for binary black holes: A Gaussian process regression approach, *Phys. Rev. D* **101**, 063011 (2020), arXiv:1903.09204 [gr-qc].
- [18] O. Gramaxo Freitas, A. Theodoropoulos, N. Villanueva, T. Fernandes, S. Nunes, J. A. Font, A. Onofre, A. Torres-Forné, and J. D. Martin-Guerrero, Deep learning powered numerical relativity surrogate for binary black hole waveforms, *Phys. Rev. D* **112**, 043026 (2025), arXiv:2412.06946 [gr-qc].
- [19] S.-C. Fragkouli, P. Nousi, N. Passalis, P. Iosif, N. Stergioulas, and A. Tefas, Deep residual error and bag-of-tricks learning for gravitational wave surrogate modeling, *Applied Soft Computing* **147**, 110746 (2023).
- [20] S. E. Field, C. R. Galley, J. S. Hesthaven, J. Kaye, and M. Tiglio, Fast Prediction and Evaluation of Gravitational Waveforms Using Surrogate Models, *Physical Review X* **4**, 031006 (2014), arXiv:1308.3565 [gr-qc].
- [21] P. Nousi, S.-C. Fragkouli, N. Passalis, P. Iosif, T. Apostolatos, G. Pappas, N. Stergioulas, and A. Tefas, Autoencoder-driven spiral representation learning for gravitational wave surrogate modelling, *Neurocomputing* **491**, 67 (2022).
- [22] G. Ashton and others, BILBY: A user-friendly Bayesian inference library for gravitational-wave astronomy, *Astrophys. J. Suppl.* **241**, 27 (2019).
- [23] A. H. Mroue *et al.*, Catalog of 174 Binary Black Hole Simulations for Gravitational Wave Astronomy, *Phys. Rev. Lett.* **111**, 241104 (2013), arXiv:1304.6077 [gr-qc].
- [24] M. Boyle *et al.*, The SXS Collaboration catalog of binary black hole simulations, *Class. Quant. Grav.* **36**, 195006 (2019), arXiv:1904.04831 [gr-qc].

- [25] M. A. Scheel *et al.*, The SXS collaboration’s third catalog of binary black hole simulations, *Class. Quant. Grav.* **42**, 195017 (2025), arXiv:2505.13378 [gr-qc].
- [26] J. Healy and C. O. Lousto, Third RIT binary black hole simulations catalog, *Phys. Rev. D* **102**, 104018 (2020), arXiv:2007.07910 [gr-qc].
- [27] J. Healy and C. O. Lousto, Fourth RIT binary black hole simulations catalog: Extension to eccentric orbits, *Phys. Rev. D* **105**, 124010 (2022), arXiv:2202.00018 [gr-qc].
- [28] K. Kiuchi, K. Kawaguchi, K. Kyutoku, Y. Sekiguchi, M. Shibata, and K. Taniguchi, Sub-radian-accuracy gravitational waveforms of coalescing binary neutron stars in numerical relativity, *Phys. Rev. D* **96**, 084060 (2017), arXiv:1708.08926 [astro-ph.HE].
- [29] H.-J. Kuan, I. Markin, M. Ujevic, T. Dietrich, K. Kiuchi, M. Shibata, and W. Tichy, The error budget of binary neutron star merger simulations for configurations with high spin, (2025), arXiv:2506.02115 [gr-qc].
- [30] M. Li, J. Wu, X. Wang, C. Chen, J. Qin, X. Xiao, R. Wang, M. Zheng, and X. Pan, Aligndet: Aligning pre-training and fine-tuning in object detection, in *Proceedings of the IEEE/CVF International Conference on Computer Vision* (2023) pp. 6866–6876.
- [31] V. B. Parthasarathy, A. Zafar, A. Khan, and A. Shahid, The ultimate guide to fine-tuning llms from basics to breakthroughs: An exhaustive review of technologies, research, best practices, applied research challenges and opportunities, arXiv preprint arXiv:2408.13296 (2024).
- [32] V. Varma, S. E. Field, M. A. Scheel, J. Blackman, L. E. Kidder, and H. P. Pfeiffer, Surrogate model of hybridized numerical relativity binary black hole waveforms, *Phys. Rev. D* **99**, 064045 (2019), arXiv:1812.07865 [gr-qc].
- [33] V. Varma, S. E. Field, M. A. Scheel, J. Blackman, D. Gerosa, L. C. Stein, L. E. Kidder, and H. P. Pfeiffer, Surrogate models for precessing binary black hole simulations with unequal masses, *Phys. Rev. Res.* **1**, 033015 (2019).
- [34] S. E. Field *et al.*, GWSurrogate: A Python package for gravitational wave surrogate models, *J. Open Source Softw.* **10**, 7073 (2025), arXiv:2504.08839 [astro-ph.IM].
- [35] F. Pedregosa, G. Varoquaux, A. Gramfort, V. Michel, B. Thirion, O. Grisel, M. Blondel, P. Prettenhofer, R. Weiss, V. Dubourg, J. Vanderplas, A. Passos, D. Cournapeau, M. Brucher, M. Perrot, and E. Duchesnay, Scikit-learn: Machine learning in Python, *Journal of Machine Learning Research* **12**, 2825 (2011).
- [36] M. A. Scheel, M. Boyle, K. Mitman, N. Deppe, L. C. Stein, C. Armaza, M. S. Bonilla, L. T. Buchman, A. Ceja, H. Chaudhary, Y. Chen, M. Corman, K. Zoltán Csukás, C. Melize Ferrus, S. E. Field, M. Giesler, S. Habib, F. Hébert, D. A. Hemberger, D. A. B. Iozzo, T. Islam, K. Z. Jones, A. Khairnar, L. E. Kidder, T. Knapp, P. Kumar, G. Lara, O. Long, G. Lovelace, S. Ma, D. Melchor, M. Morales, J. Moxon, P. James Nee, K. C. Nelli, E. O’Shea, S. Ossokine, R. Owen, H. P. Pfeiffer, I. G. Pretto, T. Ramirez-Aguilar, A. Ramos-Buades, A. Ravichandran, A. Ravishankar, S. Rodriguez, H. R. Rüter, J. Sanchez, M. Arif Shaikh, D. Sun, B. Szilágyi, D. Tellez, S. A. Teukolsky, S. Thomas, W. Throwe, V. Varma, N. L. Vu, M. Walker, N. A. Wittek, and J. Yoo, The SXS collaboration’s third catalog of binary black hole simulations, *Classical and Quantum Gravity* **42**, 195017 (2025), arXiv:2505.13378 [gr-qc].
- [37] M. Boyle and M. Scheel, The sxs package (2024).
- [38] N. Altman and M. Krzywinski, The curse(s) of dimensionality, *Nature Methods* **15**, 399 (2018).
- [39] J. Murel, What is dimensionality reduction? |ibm (2024).
- [40] Introduction to Dimensionality Reduction, section: Machine Learning.
- [41] R. Irazzad and X. Liu, A review of random forest-based feature selection methods for data science education and applications, *International Journal of Data Science and Analytics* **20**, 197 (2024).
- [42] J. Skilling, Nested Sampling, in *Bayesian Inference and Maximum Entropy Methods in Science and Engineering: 24th International Workshop on Bayesian Inference and Maximum Entropy Methods in Science and Engineering*, American Institute of Physics Conference Series, Vol. 735, edited by R. Fischer, R. Preuss, and U. V. Toussaint (AIP, 2004) pp. 395–405.
- [43] M. J. Williams, J. Veitch, and C. Messenger, Nested sampling with normalizing flows for gravitational-wave inference, *Phys. Rev. D* **103**, 103006 (2021), arXiv:2102.11056 [gr-qc]